



## Full Text View

[Volume 28, Issue 6 \(June 1998\)](#)

### Journal of Physical Oceanography

 Article: pp. 1205–1223 | [Abstract](#) | [PDF \(861K\)](#)

# Meridional Overturning and Dianeutral Transport in a z-Coordinate Ocean Model Including Eddy-Induced Advection

**Anthony C. Hirst**

*Division of Atmospheric Research, CSIRO, Aspendale, Victoria, Australia*

**Trevor J. McDougall**

*Division of Marine Research, CSIRO, Hobart, Tasmania, Australia*

(Manuscript received March 10, 1997, in final form September 22, 1997)

DOI: 10.1175/1520-0485(1998)028<1205:MOADTI>2.0.CO;2

### ABSTRACT

The present study examines the marked changes in the patterns of meridional overturning and dianeutral motion that occur upon introduction of the Gent and McWilliams (GM) scheme for eddy-induced transport into a coarse-resolution global ocean model. Results from two versions of the ocean model are compared. The first version does not have the GM scheme and uses a standard background horizontal diffusivity. The second version includes the GM scheme and has zero horizontal diffusivity. Both versions include a weak vertical diffusivity and isoneutral tracer diffusion as implemented by Cox. First, representations of the meridional overturning circulation computed via integration along (i) level, (ii) potential density, and (iii) neutral density ( $\gamma$ ) surfaces are compared. Differences between the level surface representations are similar to those noted in previous studies. Differences between the density surface representations (not previously studied) are major at high densities ( $\gamma$  or  $\sigma_\theta > 27.0$ ). The residual Deacon cell of the first version has completely vanished in the GM version. The separate direct Antarctic and deep circulation cells of the first version are fully merged in the GM version. In these respects, the solution of the GM version is broadly more consistent with that of the FRAM eddy-permitting simulation. However, introduction of the GM scheme does not aid long-standing model problems of excessive upwelling of deep water into the thermocline in the Pacific and excessive penetration of Antarctic Bottom Water into the North Atlantic. The marked differences between the versions noted above imply marked differences in the dianeutral transport of fluid. A direct calculation of dianeutral transport shows that this transport is much weaker in the Southern Ocean and in the western boundary currents in the GM run. A breakup of the dianeutral transport into components resulting from the individual model mixing processes shows that the sole factor responsible for these qualitative changes is the absence of dianeutral motion induced by horizontal diffusive fluxes in the GM version. The interior dianeutral transport in this version is characterized by widespread and gentle upward motion induced by vertical diffusive fluxes. The results are shown to be insensitive to details of the surface boundary restoration. Consequences for our understanding of (i) the role of the Deacon cell as a tracer transport mechanism and (ii) the nature of the eddy-induced transports as provided by the GM scheme are discussed. In particular, although the total effective transport in the ocean interior is nearly isoneutral in the GM case, the eddy-induced part of that transport is shown to have a

#### Table of Contents:

- [Introduction](#)
- [Model and experiments](#)
- [Results](#)
- [Discussion](#)
- [Conclusions](#)
- [REFERENCES](#)
- [TABLES](#)
- [FIGURES](#)

#### Options:

- [Create Reference](#)
- [Email this Article](#)
- [Add to MyArchive](#)
- [Search AMS Glossary](#)

#### Search CrossRef for:

- [Articles Citing This Article](#)

#### Search Google Scholar for:

- [Anthony C. Hirst](#)
- [Trevor J. McDougall](#)

## 1. Introduction

Users of coarse-resolution ocean models have traditionally controlled numerical noise by retaining a large dianeutral diffusivity (i.e., mixing across neutral surfaces). In the widely used Bryan–Cox model (Cox 1984), a horizontal diffusivity is prescribed to control numerical noise. However, there appears little justification for horizontal diffusivity in the ocean interior on physical grounds (McDougall and Church 1986). Further, recent studies show that horizontal diffusive fluxes result in serious distortion of the solution for both eddy-permitting and coarse-resolution models (Cummins et al. 1990; Böning et al. 1995; Hirst et al. 1996). Therefore, there is considerable interest in the scheme of Gent and McWilliams (1990, hereafter GM) and Gent et al. (1995), which parameterizes the adiabatic transport of oceanic tracers by mesoscale eddies, and also has the important property of allowing ocean models to run with little or no horizontal diffusivity (Danabasoglu et al. 1994; Danabasoglu and McWilliams 1995).

This paper presents an analysis of the meridional overturning and dianeutral transport<sup>1</sup> in a model that uses the GM scheme. The study is motivated, in part, by results from Hirst et al. (1996, hereafter HJM), where such issues were examined in a global ocean model without the GM scheme and with a typical value for background horizontal diffusivity. These authors calculated the meridional overturning circulation of the model via zonal integration along the model’s neutral density surfaces (McDougall 1987a). This representation of the overturning reveals the pattern of zonally integrated dianeutral transport, and HJM then split this transport into its component parts resulting from the individual diffusive mixing processes and convective adjustment. They showed that the unphysical horizontal diffusive fluxes produced a large portion of the dianeutral transport associated with the meridional overturning circulation. For example, these fluxes induced an upward dianeutral transport of more than 20 Sv through most of the range of densities in the Southern Ocean between 55° and 65°S. In contrast, the GM scheme cannot by itself induce dianeutral transport, as it is advective, not diffusive. It can only affect dianeutral transport by changing the curvature of the tracer fields, so that contributions to dianeutral transport by the remaining diffusive processes (isoneutral and vertical tracer diffusion) change, or by changing the pattern of convective mixing. Here we examine the change in meridional overturning and the pattern of dianeutral transport when the GM scheme is implemented and horizontal diffusion eliminated, thereby removing a previously major instigator of dianeutral transport. The results for the Southern Hemisphere are compared to those obtained by Döös and Webb (1994), Döös (1994), and McIntosh and McDougall (1996) for the FRAM model, which is both eddy-permitting and has very low horizontal diffusivity owing to its fine resolution. The results also shed some light on two issues currently under discussion in the literature. The first issue is whether or not the GM scheme really is a parameterization of “bolus” transport (e.g., McDougall 1991; Gent et al. 1995). The second issue concerns the importance of the Deacon cell as a tracer transport mechanism.

The paper is organized as follows. The model is described in section 2a, and the experimental details are given in section 2b. Section 2c reviews the calculation of the overturning streamfunction in isopycnal and neutral density coordinates. Section 3 presents results for the changes in the meridional overturning streamfunction and dianeutral transport between model runs with and without the GM scheme. Section 4 includes the comparison with FRAM and a discussion of the role of the Deacon cell in tracer transport.

## 2. Model and experiments

### a. Model

The global ocean model is described by Hirst and McDougall (1996). Briefly, it is based on the Bryan–Cox code (Cox 1984) and has a grid spacing of 1.6° latitude by 2.8° longitude with 21 levels in the vertical. The prescribed profile of vertical diffusivity ( $\kappa_v$ ) follows that of Bryan and Lewis (1979), where the diffusivity is near  $0.3 \text{ cm}^2 \text{ s}^{-1}$  above 1500-m depth and increases to near  $1.3 \text{ cm}^2 \text{ s}^{-1}$  below 3500-m depth. Convective mixing is simulated by setting vertical diffusivity to  $10^6 \text{ cm}^2 \text{ s}^{-1}$  in regions of static instability. A value of  $\kappa_v$  slightly larger than background is also prescribed between the upper three levels (to 80-m depth) to roughly include some surface mixing effect. Isonneutral tracer diffusion (i.e., diffusion of a tracer in the neutral direction) is included via the small angle approximation to the Redi (1982) diffusion tensor as implemented by Cox (1987). The isoneutral diffusivity  $\kappa_i$  is set at  $1 \times 10^7 \text{ cm}^2 \text{ s}^{-1}$ .

Results from two versions of the above model are presented here. The first version includes no eddy-induced transport and a horizontal background diffusivity  $\kappa_h$  of  $0.7 \times 10^7 \text{ cm}^2 \text{ s}^{-1}$ . Such a value of  $\kappa_h$  is typical of that used in global ocean models employing the Cox (1987) tracer diffusion scheme (e.g., Manabe et al. 1991; England 1993) and is required for numerical stability. It is referred to here as the “HB” version (for “horizontal background diffusion”). The second version includes eddy-induced advection according to GM and Gent et al. (1995) and no horizontal diffusivity. It is referred to here as the “GM” version. Implementation of the eddy-induced advection is as described in Hirst and McDougall (1996). An eddy-induced horizontal transport velocity ( $u_+$ ,  $v_+$ ) of the form

is added to the usual resolved-scale (or “Eulerian mean”) horizontal velocity for the purpose of tracer advection, and the sum is referred to as the “effective transport velocity.” The vertical component of the effective transport velocity is computed via continuity. In (1),  $\rho$  is the locally referenced potential density, and the parameter  $\kappa_e$  is given the value  $1 \times 10^7 \text{ cm}^2 \text{ s}^{-1}$ .

The total advection velocity of the GM method is the three-dimensional version of the zonally averaged residual-mean circulation of the atmospheric literature, and because of this direct correspondence, [McDougall and McIntosh \(1996\)](#) and [McDougall et al. \(1996\)](#) refer to the total circulation as the temporal-residual-mean (TRM) circulation. However, for now we follow present general nomenclature and refer to the total circulation as the effective transport circulation.

### *b. Experimental details*

Four simulations are examined, two for each of the above versions. The differences between the four runs are summarized in [Table 1](#). The first pair of runs are referred to as HB-1 and GM-1 and feature fairly realistic density fields<sup>2</sup> and water properties. Realistic water properties are required for the software of [Jackett and McDougall \(1997\)](#) to be used to calculate the neutral density structure (see [section 2c](#)), which is useful in the assessment of dianeutral transport. Attainment of realistic water properties in both versions despite the large difference in model physics requires differences in the details of the surface restoration imposed on temperature and salinity. The run HB-1 is simply run 1 of HJM, and uses a very short restoration timescale of 4 days, together with a significant prescribed increase in restoration salinity over parts of the Antarctic continental shelf. GM-1 uses a standard restoration timescale of 15 days [equivalent to a restoring flux of  $75 \text{ W m}^{-2} \text{ K}^{-1}$  as per [Danabasoglu and McWilliams \(1995\)](#) and many others] and restoration to unmodified [Levitus \(1982\)](#) surface values over the Antarctic continental shelf. The meridional overturning and dianeutral transport in these two runs are compared in [sections 3a–c](#). The marked qualitative differences evident are shown to result from the differing model physics and not from the differing details of the surface restoration.

It should be stressed that we do not advocate the use of enhanced restoration salinity near Antarctica (as in HB-1) as a general modeling practice. Toggweiler and Samuels (1995) have strongly criticized this practice from several points of view. In the case of HB-1, [Hirst and McDougall \(1996\)](#) showed that the enhanced Antarctic salinity plus strong restoration leads to excessive heat and freshwater fluxes over the Antarctic continental shelves. The inability of HB-type models to simulate realistic water masses with realistic surface fluxes suggests that such models have important aspects of physics that are incorrect or incomplete. The device of enhanced Antarctic salinity is used here in HB-1 only to bring the HB version to a state similar to that of the GM version, in terms of water properties, so that the physics operating at depth may be more readily compared and so that the software of [Jackett and McDougall \(1997\)](#) may be employed.

A more usual practice when comparing model versions with different physics is to specify common surface restoration conditions and examine the differences in water mass structure and other properties of the solution. This was done for the present HB and GM versions in [Hirst and McDougall \(1996\)](#) in their runs 1 and 2, which we shall refer to here as runs “HB-2” and “GM-2,” respectively ([Table 1](#)). Both runs use a surface restoration of timescale 30 days and there is no modification to Antarctic salinities. Under this common restoration, the two model versions yield very different subsurface densities, with that for GM-2 being much the more realistic ([Hirst and McDougall 1996](#)). In [section 3d](#), we examine the meridional overturning and dianeutral transport of these two runs to establish the generality of the differences between the HB-1 and GM-1 solutions found in [sections 3a–c](#). However, neither HB-2 nor GM-2 yield sufficiently realistic density fields for accurate use of Jackett and McDougall’s method over the entire model domain (see [section 2c](#)). Therefore, the analysis of [section 3d](#) uses potential (rather than neutral) density as the vertical coordinate.

The analysis of meridional overturning in potential or neutral density coordinates is made considerably more complicated if temporal fluctuations (e.g., an annual cycle) are present in the solution because such fluctuations in velocity and density introduce inaccuracies in the calculated mean overturning unless sampling is very frequent. Therefore, all four runs are performed using temporally constant upper boundary conditions. The model is forced with the climatological annual-mean wind stress of [Hellerman and Rosenstein \(1983\)](#). Surface temperature ( $T$ ) and salinity ( $S$ ) are restored toward climatological wintertime values, as recommended by [Williams et al. \(1995\)](#). [Hirst and Cai \(1994\)](#) found that such a configuration yielded subsurface temperature/salinity fields and meridional overturning that were similar to those occurring under a full annual cycle of surface forcing, provided that the late winter surface  $T$  and  $S$  fields of the cyclic run closely matched those of the constant wintertime run.

The  $T$  and  $S$  restoration fields are taken from the late winter (Mar–Sep) surface climatology of [Levitus \(1982\)](#). Minor modifications to the restoration fields are made in the northern Greenland Sea, the central Labrador Sea, and the Gulf of Lyons to better conform to observed seasonal extrema (see [Hirst and McDougall 1996](#)). In the case of HB-1, additional modification of the  $S$  field is made over the Antarctic shelves as noted above.

The model is run to quasi-equilibrium of the thermohaline fields using the acceleration techniques of [Bryan \(1984\)](#). The time step for  $\theta$  and  $S$  in the upper ocean is 3 days, increasing to 8 days at the lowest model level. The run is completed when the trends in  $\theta$  and  $S$  averaged globally for each model level drop below  $1 \times 10^{-2} \text{ }^\circ\text{C}$  per century and  $2 \times 10^{-3}$  psu per century.

[Döös and Webb \(1994\)](#), [McIntosh and McDougall \(1996\)](#), and HJM discuss computation of the overturning streamfunction in potential or neutral density coordinates. Briefly, let  $\xi(\phi, \lambda, z)$  be any variable that varies monotonically with depth ( $z$ ), where  $\lambda$  and  $\phi$  are latitude and longitude. We define a streamfunction

$$\psi(\lambda, \xi) = \int \int_{z(\phi, \lambda, \xi)}^0 v(\phi, \lambda, z') a \cos \lambda dz' d\phi, \quad (2)$$

where  $a$  is the earth's radius, and  $\mathbf{v}$  is either the effective transport, Eulerian-mean, or eddy-induced transport velocity in the meridional. The integration (2) is performed by first integrating the meridional velocities from the upper-ocean surface to the depth of the appropriate  $\xi$  surface, and then integrating zonally either about the globe or across a closed basin. Thus, meridional transport between two  $\xi$  surfaces at a particular latitude is given by the difference in the streamfunction. For steady-state solutions, as here, a difference in the streamfunction at different latitudes but at the same  $\xi$  value indicates the flux of water across that  $\xi$  surface. The present study shows streamfunctions for  $\xi = z$  (i.e., the standard level-surface integration), for  $\xi = \sigma_\theta$  and  $\sigma_3$  [the potential density referenced to the surface and to 3000-db pressure (depth  $\sim 3$  km), respectively], and for  $\xi = \gamma$  [the neutral density coordinate of [Jackett and McDougall \(1997\)](#)].

A major drawback of a potential density coordinate system results from the ambiguity in the choice of reference level. The potential density  $\sigma_\theta$  represents the upper-ocean density structure closely and the deep ocean density structure poorly, while  $\sigma_3$  does conversely. This ambiguity can lead to difficulties in interpreting, for example, an overturning streamfunction calculated in potential density coordinates. The neutral density coordinate minimizes such ambiguity and provides a representation of the density structure relevant at all depths. Water on a neutral surface remains on that surface unless it has its buoyancy changed as a result of mixing or surface buoyancy flux. Changes in buoyancy result in dianeutral transport, or flow across neutral surfaces. [McDougall \(1987a,b\)](#) has shown that buoyancy changes and associated dianeutral transport may be readily separated into parts resulting from the different mixing processes. It is therefore possible to interpret the overturning cells of the  $\gamma$  coordinate streamfunction in terms of the action of these mixing processes.

An advantage of potential density coordinates is that potential density fields can always be readily calculated for any model solution. In contrast, computation of the neutral density structure from first principles involves tracing many neutral surfaces through the model domain [e.g., using the method of [Reid \(1994\)](#)], and this proves to be very difficult for an ocean domain as complicated as the World Ocean. However, the  $\gamma$  field may now be calculated (to within known error bounds) in a practical manner via the scheme of [Jackett and McDougall \(1997\)](#). Under this scheme, each model  $T/S$  point is assigned a neutral density (or  $\gamma$ ) value obtained by finding the position on a cast of [Levitus \(1982\)  \$T/S\$  climatological data that corresponds neutrally to the model  \$T/S\$  point and then by reading off the precomputed  \$\gamma\$  value for that position. Points on separate model "casts" that have the same  \$\gamma\$  value then lie on the same neutral density surface. A potential error in the assigned  \$\gamma\$  value arises from the differences between the model cast and the Levitus cast. The upper bound on this error is proportional to  \$\Delta p \Delta \theta\$ , where  \$\Delta p\$  is the pressure difference and  \$\Delta \theta\$  the potential temperature difference between points on the model and Levitus casts that correspond neutrally. Thus, the less realistic the model  \$\theta\$  and density fields, the larger the error bound.](#)

Since the above errors in  $\gamma$  could have a significant effect on the overturning streamfunction, we test the reliability of the streamfunction as follows. Two adjusted  $\gamma$  fields are created, in the first case by replacing the calculated  $\gamma$  with its upper bound at points with northward velocity and with its lower bound at points with southward velocity and in the second case by the converse. Overturning streamfunctions are then computed using these two adjusted  $\gamma$  fields, and the original streamfunction (computed with the unadjusted  $\gamma$  field) is deemed unreliable in regions where streamfunctions from the adjusted  $\gamma$  fields differ from each other by more than a certain tolerance. The  $\gamma$  streamfunctions for the HB-1 and GM-1 solutions pass this test over the entire density–latitude domain, using a tolerance of 2 Sv. The  $\gamma$  streamfunction for GM-2 fails this test at some high density classes in the Southern Ocean, where departures from observed potential density are regionally up to  $-0.2 \text{ kg m}^{-3}$ , while that for HB-2 fails the test over high density classes at all latitudes and for some lower density classes in the Southern Ocean. Therefore, we do not use the  $\gamma$  streamfunctions for GM-2 and HB-2 in this study.

### 3. Results

#### a. Overturning streamfunctions

[Figure 1](#) compares the overturning streamfunctions for the GM-1 and HB-1 solutions, calculated using the standard level-surface integration  $\psi(\lambda, z)$ . The effective transport velocity is used for the GM-1 calculation. Near-surface cells in both solutions include a Deacon cell (centered near 50°S) and cells associated with the south and north subtropical gyres. The imprint of the Atlantic overturning circulation is also evident in both solutions (centered near 40°–55°N at depth roughly 1 km). Some marked differences are evident between the solutions. First, the Deacon cell in the GM-1 solution is very much weaker and shallower than in HB-1. Second, HB-1 shows two deep counterclockwise cells, an Antarctic cell centered near 65°S and depth 1.7 km and a deep cell between roughly 20° and 50°S and at a depth of 3.5 km. In the GM-1 solution, these two cells merge, with a weakened Antarctic cell seen merely as an extension of the deep cell (now centered at 40°S and



depth 3.2 km). We refer to this combined cell as the “Antarctic-deep” cell. The above differences between GM-1 and HB-1 are broadly consistent with those found in similar comparisons elsewhere (e.g., Danabasoglu and McWilliams 1995; [England and Hirst 1997](#)).

The effective transport velocity of the GM-1 solution may be split into Eulerian-mean and eddy-induced components, and the overturning streamfunctions for the separate components are shown in [Fig. 2](#). The Eulerian-mean transport streamfunction ([Fig. 2a](#)) displays a strong and deep Deacon cell separating a weak Antarctic cell and a deep cell. The pattern for the eddy-induced transport ([Fig. 2b](#)) is dominated by a direct cell in the Southern Ocean, which has flow in the opposite sense to the Deacon cell. This latter cell more than cancels the Deacon cell at depths greater than 1 km ([Fig. 1a](#)). The patterns in [Fig. 2](#) are similar to those found in other modeling studies (e.g., [Danabasoglu and McWilliams 1995](#)). The eddy-induced transport pattern is also similar to that given by the GM scheme for the observed ([Levitus 1982](#)) density field ([Gent et al. 1995](#)).

[Figure 3](#) shows the overturning streamfunctions for the effective transport velocity of GM-1 for the Atlantic and Indian/Pacific Oceans, separately. The patterns are mostly similar to those for HB-1 (HJM’s [Fig. 2](#)). The peak streamfunction value of the Atlantic overturning circulation (at about 40°N and depth 0.9 km) is about 40% weaker in GM-1 than in HB-1, and the deep Atlantic outflow is shallower by about 500 m. These changes are broadly consistent with those found in other global ocean models that feature a realistic Greenland–Scotland sill depth ([England and Hirst 1997](#), manuscript submitted to *J. Phys. Oceanogr.*; S. B. Power 1995, personal communication).

We now examine the overturning streamfunction for the GM-1 solution, as calculated by zonal integration along potential density surfaces. Attention is restricted to the streamfunction of the effective transport velocity since this is the velocity that advects density and tracers. The overturning streamfunction  $\Psi(\lambda, \sigma_\theta)$  is shown in [Fig. 4a](#). Shading indicates the densities that outcrop at each latitude circle, where water density may be strongly altered by surface heat or freshwater flux. Densities that do not outcrop anywhere in the latitude circle are referred to as “fully interior” densities. In [Fig. 4a](#), “upward” transport implies a diapycnal transport toward lesser densities in the zonal integration. The twin subtropical gyre cells dominate the circulation at densities less than 26.8 and are almost unchanged from those of HB-1 (HJM’s [Fig. 3](#)). The flows associated with these cells are discussed in some detail by [Döös \(1996\)](#) and HJM.


[Figure 4](#) also shows two representations of the high density portion of the overturning streamfunction. The first ([Fig. 4b](#)) is an expanded view of  $\Psi(\lambda, \sigma_\theta)$  for the high density range, and the second ([Fig. 4c](#)) shows  $\Psi(\lambda, \sigma_3)$  for a roughly equivalent range of densities. The Atlantic overturning circulation is clearly evident in both representations, with maximum streamfunction now centered near 55°N (compared to 40°N in [Fig. 1a](#)). The Antarctic-deep cell of [Fig. 1a](#) is also evident near  $\sigma_\theta = 27.8$  ([Fig. 4b](#)) and near  $\sigma_3 = 41.7$  ([Fig. 4c](#)). The weak Deacon cell of [Fig. 1a](#) has completely vanished in both representations.



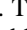


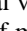
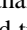
[Figure 4](#) again demonstrates the limitations of using potential density referenced to a fixed pressure for this kind of analysis, as discussed by HJM. The artificial superposition of the Antarctic bottom outflow and Atlantic deep outflow is evident in the  $\sigma_\theta$  representation ([Fig. 4b](#)), while the artificial enhancement of a cell involving near-surface flows (centered at 50°S and  $\sigma_3 = 40.8$ ) is evident in the  $\sigma_3$  representation ([Fig. 4c](#)). Such artifacts are avoided by the use of neutral density.


The overturning streamfunction in  $\gamma$  coordinates [ $\Psi(\lambda, \gamma)$ ] is shown in [Fig. 5](#). [Figure 5a](#) shows the streamfunction for GM-1 over the full  $\gamma$  range, and [Fig. 5b](#) shows an expanded view of the high  $\gamma$  range. Similar to [Fig. 4](#), “upward” and “downward” transport implies net diapycnal transport across the  $\gamma$  surfaces in the zonal integration. The analysis extends only to 60°N, which is close to the northern limit attainable by Jackett and McDougall’s software. The overall pattern is as inferred from [Fig. 4](#). Readily seen are the subtropical gyre cells at  $\gamma$  less than 26.8, the Atlantic overturning cell (centered at 55°N and  $\gamma = 27.75$ ), and the Antarctic-deep cell (centered near  $\gamma = 28.2$ ).

The subtropical gyre cells of GM-1 are little changed from those of HB-1 (HJM’s [Fig. 5](#)). However, the streamfunctions for the two runs display major qualitative differences at higher  $\gamma$ . For comparison, the high  $\gamma$  portion of the HB-1 streamfunction is reproduced in [Fig. 5c](#). The HB-1 solution features a very strong Antarctic cell with a major upward diapycnal flow of about 25 Sv on the cell’s northern flank at about 60°S. HJM showed that this diapycnal transport is sustained by horizontal diffusive flux of heat and salt, which cannot occur in the GM-1 case as the horizontal diffusivity is set to zero. Consistent with this, no corresponding upward flow is evident in the GM-1 case. This major upward flow in the HB-1 case is balanced on the southern flank of the Antarctic cell by similarly strong downward diapycnal flow. [Hirst and McDougall \(1996\)](#) examined the implied surface fluxes in HB-1 and showed that extremely large surface heat and freshwater losses occur in this run over the Antarctic continental shelves. These heat and freshwater losses are sufficient to explain the density gain associated with the downward branch of the Antarctic cell. If such density gain is not forced to occur (e.g., as in HB-2) then rapid density loss ensues from the circumpolar waters leading eventually to unrealistic bottom water properties. In the GM-1 case, there is no massive density loss near 60°S, and surface fluxes and density gain adjacent to Antarctica are relatively modest and probably much more realistic (e.g., [Jacobs et al. 1985](#)).

The HB-1 case also displays downward diapycnal transport near 40°S, which gives rise to the downward branches of the residual Deacon cell (centered at 45°S and  $\gamma = 27.7$ ) and the deep cell (centered at about 25°S and  $\gamma = 28.1$ ). HJM showed that the associated density gain also results from horizontal diffusive fluxes. Consistent with this, no such downward transport is evident in the GM-1 case ([Fig. 5b](#)). Thus, the complete absence of a residual Deacon cell and the merging of


the Antarctic and deep cells in the  $\gamma$  representation for the GM-1 case is consistent with the lack of horizontal diffusivity therein. Over most of the fully interior domain in the GM-1 case (i.e., the area below the shaded region in [Figs. 5a and 5b](#) ) , the dianeutral transport appears gentle and upward, as might result from gradual water mass modification by a weak vertical diffusivity.

Just as the level-surface overturning streamfunction of the effective transport velocity can be decomposed into Eulerian-mean and eddy-induced components (as shown in [Fig. 2](#) ) , the same decomposition can be applied in density coordinates. This is done by calculating the streamfunction, [\(2\)](#), using either the Eulerian-mean or the eddy-induced velocity separately. The results for GM-1 over the high density range are shown in [Fig. 6](#) ) , and the sum of these two panels yields the streamfunction of the effective transport velocity shown in [Fig. 5b](#) ) . The eddy-induced velocity exhibits a substantial dianeutral circulation in the Southern Ocean ([Fig. 6b](#) ) . The sense and latitudinal extent of this circulation are consistent with that shown for the level-surface integration in [Fig. 2b](#) ) . Most of the dianeutral volume transport of the eddy-induced velocity ([Fig. 6b](#) ) is balanced by the dianeutral volume transport of the Eulerian-mean velocity component ([Fig. 6a](#) ) , which exhibits a maximum dianeutral transport of more than 11 Sv in a pattern that broadly resembles a substantial Deacon cell. At  $\gamma < 26.8$ , the streamfunction for the eddy-induced transport diminishes rapidly with decreasing density, and so is not shown.

The GM scheme was originally motivated as a parameterization of the bolus transport, which is the transport caused by the unresolved temporal correlations between the thickness between neutral surfaces and the horizontal velocity vector. Bolus transport is directed along density surfaces so that if the bolus transport were zonally integrated along density surfaces, the integrated bolus transport would continue to be aligned along density surfaces. Clearly, the eddy-induced transport in [Fig. 6](#) ) does not have this characteristic. Whatever the initial motivation of the GM scheme, the practicalities of constructing such a scheme for a height coordinate model ensured that the resulting eddy-induced transport is not the bolus transport. However, recent theoretical work (McDougall and McIntosh 1996) has shown that the eddy-induced transport of the GM scheme accounts for not only the bolus transport but also transport resulting from the difference between the velocity averaged on density surfaces and at fixed height, and that this alternative interpretation does allow for dianeutral eddy-induced transport.

### *b. Thermodynamics of meridional cells*

According to [McDougall \(1987b\)](#), the dianeutral velocity in the ocean interior may be decomposed into separate parts resulting from the individual mixing processes. In the model, these processes include vertical tracer diffusion, cabbeling and thermobaricity associated with isoneutral tracer diffusion, and convective mixing. Both versions of the model also include the unphysical dianeutral mixing that occurs when the slope of the model neutral surface exceeds the maximum allowed slope for the isoneutral tracer diffusion scheme. Finally, the HB model version includes the unphysical horizontal diffusion.

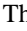

HJM decomposed the zonally integrated dianeutral velocity for HB-1 into its component parts to determine the thermodynamic processes responsible for the cells evident in the  $\gamma$  representation of the overturning streamfunction. The same procedure is used here to examine the thermodynamics of the dianeutral transport evident in [Fig. 5](#) ) for the GM-1 case. First, the zonally integrated dianeutral velocity ( $\langle e \rangle$ ) may be written ([Killworth and Nanneh 1994](#))

$$\langle e \rangle = \int_{2\pi} \mathbf{V} \cdot \hat{\rho} a \cos \lambda \, d\phi \quad (3a)$$

$$= \int_{2\pi} \frac{\mathbf{V} \cdot \nabla_3 \rho}{|\nabla_3 \rho|} a \cos \lambda \, d\phi \quad (3b)$$

$$= \int_{2\pi} \frac{\alpha \mathbf{V} \cdot \nabla_3 \theta - \beta \mathbf{V} \cdot \nabla_3 S}{|\nabla_3 \rho| / \rho} a \cos \lambda \, d\phi, \quad (3c)$$

where  $\rho$  is the locally referenced potential density,  $\hat{\rho}$  is the dianeutral unit vector,  $\nabla_3$  and  $\mathbf{V}$  are the three-dimensional gradient operator and effective transport velocity vector, and  $\alpha$  and  $\beta$  are the locally referenced expansion coefficients for potential temperature ( $\theta$ ) and salinity ( $S$ ). The zonally integrated dianeutral velocity in the model is estimated via evaluation of [\(3c\)](#), and details of the numerical procedure are given in HJM.<sup>3</sup> The calculation of  $\langle e \rangle$  via [\(3c\)](#) is useful because it allows direct breakup of  $\langle e \rangle$  into its thermodynamic components. This follows because the numerator of [\(3c\)](#) is simply the advective density tendency, which must be exactly balanced in the steady-state solution by density tendencies resulting from surface fluxes or interior mixing processes.

Evaluation of  $\langle e \rangle$  via [\(3c\)](#) is prone to truncation error in the vicinity of convective instability, where the numerator and/or denominator in [\(3c\)](#) may change rapidly on the gridpoint scale ([Killworth and Nanneh 1994](#); HJM). Thus, [\(3c\)](#) is not useful at densities that intersect the surface convective mixed layer (i.e., the lightly shaded region in [Fig. 5](#) ) . The remainder of [section 3b](#) therefore examines only the dianeutral transport at fully interior densities (i.e., beneath the shaded region in [Fig. 5](#) ) , where stratification is almost everywhere stable.

[Figure 7](#) shows the pattern of total dianeutral transport as calculated via (3c) for the surface ocean the GM-1 case. Units are Sverdrups per degree latitude, to assist in comparison with [Fig. 5](#). Positive values indicate reduction of density in the direction of flow and are reflected as “upward” transport in [Fig. 5](#). Large positive values occur between 20°N and 20°S at  $\gamma < 26.5$ , corresponding to the rising branches of the subtropical gyre circulation. The pattern here is very similar to that occurring in HB-1 (HJM’s [Fig. 7a](#)). At greater density ([Fig. 7b](#)), the fully interior ocean domain is dominated by general weak upward transport. In contrast, the HB-1 case (HJM’s [Fig. 7b](#)) displays prominent bands of dianeutral transport at about 60°S (upward), 40°S (downward), and 20°S (upward), and 20°N (upward), which extend across a large range of  $\gamma$ . The former two are clearly evident in the  $\gamma$  streamfunction for HB-1 ([Fig. 5c](#)) as the upward branch of the Antarctic cell and the downward branches of the residual Deacon cell and deep cell.

Following [McDougall \(1987b\)](#), the model dianeutral velocity ( $e$ ) may be broken into components that result from flux divergence of heat and  $S$  associated with vertical diffusion ( $e_{\text{vdiff}}$ ), cabbeling and thermobaricity associated with true isoneutral tracer diffusion ( $e_{\text{idiff}}$ ), diffusion occurring via the isoneutral tracer diffusion scheme where the neutral surface slope is in excess of the allowed mixing slope ( $e_{\text{slope}}$ ) and convective adjustment. HJM also included a component for horizontal diffusion. At depths below the surface mixed layer, we may write for the GM version

$$e = e_{\text{vdiff}} + e_{\text{idiff}} + e_{\text{slope}} + e_{\text{res}}$$

$$= \frac{\alpha(\kappa_v \theta_z) - \beta(\kappa_v S_z)}{|\nabla_3 \rho|/\rho} + \delta \left( \frac{\alpha R(\kappa_i, \theta) - \beta R(\kappa_i, S)}{|\nabla_3 \rho|/\rho} \right) + (1 - \delta) \left( \frac{\alpha R(\kappa_i, \theta) - \beta R(\kappa_i, S)}{|\nabla_3 \rho|/\rho} \right) + e_{\text{res}} \quad (4)$$

*(Click the equation graphic to enlarge/reduce size)*

where  $R$  is the rotation tensor used by the [Cox \(1987\)](#) isoneutral tracer diffusion scheme and  $\delta$  equals unity if the neutral surface slope is less than 1:100 and zero otherwise. The first three terms on the right-hand side may be estimated directly from the model fields. A residual ( $e_{\text{res}}$ ) is also calculated, which includes the effect of convective adjustment plus any errors, for example, resulting from the presence of transients in the solution. The component velocities are then integrated zonally along surfaces of constant  $\gamma$ .

[Figure 8](#) shows the portion of the total dianeutral transport ([Fig. 7](#)) in the GM-1 case that results from each of the above components. Only the high  $\gamma$  range is shown. For this range of  $\gamma$ , modest contributions made by the last three terms of (4) are restricted to high latitudes, to densities fairly close to the surface range, and to the region near the in-mixing of Mediterranean Water. However, over the large majority of the fully interior domain, the vertical diffusion component is the only significant contributor to the dianeutral transport, and its contribution is characterized by weak large-scale upward transport ([Fig. 8a](#)). The next most substantial contribution is by the isoneutral tracer diffusion component ([Fig. 8b](#)), and this contribution is downward, as expected for cabbeling ([McDougall 1987b](#)). The contribution resulting from the slope limitation ([Fig. 8c](#)) is very small over most of the domain. Nevertheless, this contribution is unphysical, and it is recommended that some scheme to reduce  $\kappa_i$  in steeply sloping regions (e.g., [Gerdes et al. 1991](#); [Danabasoglu and McWilliams 1995](#)) be used to satisfy the numerical constraint instead of the standard slope limitation technique. The residual term ([Fig. 8d](#)) is negligible over almost the entire domain, reflecting the near absence of convection at interior densities and the near stationarity of the solution.

At  $\gamma < 26.8$ , the total transport for GM-1 ([Fig. 7a](#)) results almost entirely from the vertical diffusion component, as is also the case for HB-1 (see HJM’s [Figs. 7–9](#)). Thus, the thermodynamics of the subtropical gyre cells has not changed significantly between the runs. The dominant role of vertical diffusion in dianeutral density flux and transport in this low  $\gamma$  domain is consistent with the results of [McWilliams et al. \(1996\)](#), who examined mechanisms of heat transport across isothermal surfaces of  $\theta > 19^\circ\text{C}$  (approximately  $\gamma < 25.0$ ) in their global ocean model, which includes the GM scheme.

The chief difference overall between the dianeutral transport in the HB-1 and GM-1 cases is the absence of the component caused by horizontal diffusion in the GM-1 case. There is relatively little change in the other components. The vertical diffusion component ([Fig. 8a](#)) is slightly larger over the density range  $26.8 < \gamma < 27.8$  than in HB-1 (HJM’s [Fig. 8b](#)), which may reflect increased curvature of the density field associated with the sharper pycnocline in the GM-1 case ([Danabasoglu and McWilliams 1995](#); [Hirst and McDougall 1996](#)). This increase in  $e_{\text{vdiff}}$  partly compensates for the loss of global scale upwelling induced by horizontal diffusive fluxes in HB-1. For example,  $e_{\text{vdiff}}$  and  $e_{\text{hdiff}}$  contribute 7 and 6 Sv, respectively, to the net 12-Sv upward transport across the  $\gamma = 27.7$  surface between 35°S and 50°N, in HB-1 (HJM). In the GM-1 case,  $e_{\text{vdiff}}$  contributes 9 Sv to the corresponding net upward transport of 8.5 Sv.

We note a discrepancy between the total dianeutral transport calculated via (3) and the dianeutral transport indicated by the overturning streamfunction. [Figure 5b](#) shows downward transport between 50° and 65°S at a  $\gamma$  of about 28.25, corresponding to an interior ocean portion of the downward branch of the Antarctic deep cell accounting for 4-Sv dianeutral transport. Yet [Fig. 7b](#) shows no net downward transport north of 60°S. According to [Fig. 7b](#), the center of the cell should be near 60°S, rather than at about 45°S as seen in [Fig. 5b](#). There are several possible causes of such a discrepancy; however, we suspect that errors in the calculated  $\gamma$  field are a likely contributor. Modest errors in the  $\gamma$  field could substantially affect the streamfunction of [Fig. 5b](#) by incorrectly recasting isoneutral flow as dianeutral. In contrast, [Fig. 7b](#) is unlikely to be much affected by such errors because the dianeutral velocity is calculated using the model’s locally referenced potential density gradients, and  $\gamma$  is used only for zonal integration. To check the assigned  $\gamma$  values, we traced several dozen neutral surfaces northward from the Ross and Weddell Sea shelves and also southward from the deep

ocean toward Antarctica, using software provided by D. R. Jackett and T. J. McDougall (1996, personal communication), which tracks individual neutral surfaces and is independent of the  $\gamma$  calculation routine. We checked this software by writing an alternative code to track neutral surfaces from model level to level using the potential density referenced to the midpoint between the levels, as given by the model equation of state (after Reid 1994). The two tracing methods gave almost identical trajectories. However, some of these trajectories diverged significantly from the trajectories of constant  $\gamma$  values, and this divergence is, cumulatively over several grid points, substantially larger than can be explained by the assigned error bars on  $\gamma$ . The probable explanation is that the error bars on  $\gamma$  are determined by a local calculation, whereas in some circumstances these errors can accumulate when tracing a surface from east to east. The problem seems to occur only in the region  $\gamma > 28.2$ , between 50°S and the Antarctic continental slope. Elsewhere, very close agreement was obtained between constant  $\gamma$  and directly computed trajectories. In contrast to the  $\gamma$  representation of the streamfunction (Fig. 5b), all potential density representations show the Antarctic-deep cell centered between 55° and 60°S regardless of reference level (e.g., Fig. 4), and this agrees more closely with Fig. 7b.

### c. Horizontal pattern of dianeutral velocity

HJM examined the horizontal pattern of dianeutral velocity across several  $\gamma$  surfaces relevant to the circulation features evident in the HB-1 streamfunction. Large regional variations of dianeutral velocity on the 27.7, 27.9, and 28.1 surfaces were shown to be induced by horizontal diffusive fluxes. Such large regional variations are not evident in the GM-1 case. As an example, Fig. 9 shows the total dianeutral velocity across the  $\gamma = 27.9$  surface in the Atlantic Ocean, for HB-1 and GM-1. The pattern of total dianeutral velocity for HB-1 (Fig. 9a) is very similar to that of the horizontal diffusion component alone (HJM's Fig. 12) and features a band of strong upward dianeutral velocity stretching along the North American coast with a weaker band of downward dianeutral velocity farther offshore. In comparison, the GM-1 pattern (Fig. 9b) shows a relatively broad band of weak upward dianeutral velocity over the western portion of the North Atlantic. The vertical diffusion component contributes  $\sim 0.1 \times 10^{-6} \text{ m s}^{-1}$  to the dianeutral velocity over this region. Unphysical mixing resulting from the slope limitation of the isoneutral tracer diffusion scheme makes a larger contribution ( $\sim 0.5 \times 10^{-6} \text{ m s}^{-1}$ ) at several locations adjacent to the coast, notably near 30° and 48°N. However, even in these locations, the total dianeutral velocity is smaller than in the HB-1 case by about a factor of 4. To compare the overall upward dianeutral transports along the western basin margin, the fields of Fig. 9 are integrated between 20° and 50°N over the coastal zones of upward motion (which is defined to include all areas of positive dianeutral velocity within 20° longitude of the western terminus of the  $\gamma = 27.9$  surface). The resulting dianeutral transport is much larger for HB-1 (4.5 Sv) than for GM-1 (1.1 Sv), as expected based on HJM's analysis (also Veronis 1975; Böning et al. 1995; Gough and Lin 1995).

The other significant difference between the cases in Fig. 9 is the difference in downward dianeutral velocity near the Strait of Gibraltar. This difference simply results from the  $\gamma = 27.9$  surface being about 400 m shallower in GM-1 than in HB-1, which places it within the outmixing zone of dense Mediterranean Water in the former case.

### d. Comparison with other runs

The approach above has been to compare model runs with different physics but similar water mass properties, achieved by use of different surface restoration parameters. A more conventional approach is to compare model runs with different physics but using the same restoration parameters, and this may lead to very different water mass properties. We therefore check, as far as is possible, the robustness of the above results by examining the solutions of Hirst and McDougall's (1996) principal model runs, here denoted HB-2 and GM-2, which use common restoration parameters. These two runs yield very disparate water mass properties, with deep water in HB-2 being insufficiently dense by typically  $0.4 \text{ kg m}^{-3}$ , while that in GM-2 was much more realistic.

The overturning streamfunctions  $\Psi(\lambda, z)$  for GM-2 and HB-2 are very similar to those of GM-1 and HB-1 (Fig. 1), respectively, and are not shown. The largest difference between the respective runs amounts to a 30% decline in the strength of the Antarctic cell from HB-1 to the more weakly forced HB-2.

Figure 10 shows the overturning streamfunction  $\Psi(\lambda, \sigma_3)$  for GM-2 and HB-2. The streamfunction for GM-2 (Fig. 10a) is almost identical to that for GM-1 (Fig. 4c). The streamfunction for HB-2 (Fig. 10b) is qualitatively similar to that for HB-1 (HJM's Fig. 4). Evident in Fig. 10b are the residual Deacon cell (centered at  $\sigma_3 = 40.9$  and 42°S) and the separate deep ( $\sigma_3 = 41.15$  and 25°S) and Antarctic ( $\sigma_3 = 41.35$  and 65°S) cells. The Antarctic cell has nearly the same intensity as that of HB-1 (30 Sv), but extends over a much smaller range of density (roughly  $0.2 \text{ kg m}^{-3}$ , compared to  $0.5 \text{ kg m}^{-3}$  for HB-1). This small range of density reflects the extremely weak stratification found generally south of 60°S in HB-2 and is also consistent with the much reduced buoyancy forcing in HB-2 relative to that in HB-1 (Hirst and McDougall 1996). The extensive areas of negative streamfunction centered near  $\sigma_3 = 40.6$  and 50°S in Figs. 10a and 10b again appear to be largely artificial, mostly vanishing in the  $\sigma_\theta$  streamfunction representation.

An analysis of the dianeutral transport similar to that in section 3b was performed for all above runs, but using surfaces of  $\sigma_3$  and  $\sigma_\theta$  for the zonal integration instead of  $\gamma$ . Results for all runs with the GM and HB model versions were respectively similar to those shown in section 3b for GM-1 and HB-1. Therefore, the marked differences between the meridional overturning and dianeutral transports in the GM and HB versions appear insensitive to details of the surface restoration scheme.



## 4. Discussion

### a. Comparison with FRAM

The meridional overturning streamfunctions for the GM model version are compared here to those obtained for the eddy-permitting FRAM Southern Ocean model by [Döös and Webb \(1994\)](#) and [McIntosh and McDougall \(1996\)](#). The FRAM solution has its significant limitations, in particular the shortness of the integration which precludes the establishment of a truly equilibrium state. However, it is the only eddy-permitting solution involving the Southern Ocean for which work comparable to that in [section 3](#) has been published. [Gent and McWilliams \(1996\)](#) have recently discussed some common aspects of the FRAM and the GM-1 solutions, in particular the behavior of the Deacon cell. The following elaborates on their comparison.

We first compare the level-surface streamfunction for FRAM and GM-1. The calculation of this streamfunction for an eddy-permitting model involves zonal integration and temporal averaging of velocity at a fixed depth that eliminates perturbation velocities; thus eddy-induced transport is not included in the streamfunction. Therefore, the level-surface streamfunction for an eddy-permitting model (e.g., [Fig. 2](#) of [Döös and Webb 1994](#)) should be compared to that for the Eulerian-mean velocity component of a coarse-resolution model (e.g., the present [Fig. 2a](#)). A comparison of the above figures shows that both feature a strong Deacon cell, a strong deep cell, and weak circulation near Antarctica. One marked difference is that the extension of the Atlantic overturning cell into the Southern Ocean appears very strong in FRAM, but very weak in the present GM-1 run.

The density surface streamfunction calculation for an eddy-permitting model involves zonal integration, then temporal averaging of transports between adjacent density surfaces, which thus captures the eddy-induced transports. Therefore, a density-surface representation for an eddy-permitting model [e.g., [Fig. 3](#) of [McIntosh and McDougall \(1996\)](#)] should be compared to that for the effective transport velocity of a coarse-resolution model (e.g., [Figs. 5a,b](#)). The above figures show that neither the FRAM nor the GM-1  $\gamma$  streamfunction exhibits a residual Deacon cell in contrast to the HB-1 run ([Fig. 5c](#)).

[Gent and McWilliams \(1996\)](#) discuss the fact that a Deacon cell cannot exist in the  $\gamma$  streamfunction of an adiabatic flow. This is because the  $\gamma$  streamfunction is constrained to be independent of latitude ( $\lambda$ ) over the range of ( $\lambda$ ,  $\gamma$ ) for which the adiabatic assumption holds, since no transport through a  $\gamma$  surface is possible, and hence any net meridional transport above or below that surface is conserved. In a model where surface buoyancy fluxes are significant but where the ocean interior is adiabatic, the streamfunction may display diapycnal transport at outcropping densities but the  $\gamma$  streamfunction must be meridionally invariant at fully interior densities. Such a case appears relevant to the FRAM model, where there is substantial diapycnal transport at outcropping densities and large but (approximately) meridionally constant streamfunction values at fully interior densities.

In the case of GM-1, the  $\gamma$  streamfunction is very small over a large range of densities ( $27.2 < \gamma < 27.9$ ) from the interior margin of the outcropping densities northward to  $30^{\circ}$ – $35^{\circ}$ S ([Figs. 5a,b](#)). This pattern resembles that for the situation where the zonally integrated surface buoyancy flux is zero and the interior is adiabatic, whereby it follows from the above that the  $\gamma$  streamfunction must also be zero at fully interior densities. For GM-1, [Fig. 8](#) does show significant and opposing contributions to diapycnal transport from vertical and isopycnal tracer diffusion just beneath the outcropping densities, and a surface buoyancy flux calculation over the density band  $27.3 < \gamma < 27.8$  in the Southern Ocean does yield a modest net buoyancy flux to the ocean equivalent to the input of  $+0.12 \text{ m yr}^{-1}$  freshwater. In GM-1, these diabatic effects largely cancel to yield small net diapycnal transport at outcropping and near-outcropping densities, and, consequently, near-zero streamfunction values, which extend well north into the nearly adiabatic interior.

While the FRAM and GM-1 solutions are similar in many respects, two discrepancies are notable. First, the abovementioned difference in the net near-surface diapycnal transport in the Southern Ocean is part of a more fundamental discrepancy. Namely, the FRAM  $\gamma$  streamfunction shows a strong extension of the Atlantic overturning cell into the Southern Ocean, whereas [Fig. 5b](#) shows only a very weak extension of this cell. This discrepancy results from a composite of discrepancies in the individual Atlantic and Indian/Pacific basins. [Döös \(1994\)](#) provides level-surface overturning streamfunctions for the separate ocean basins (between  $24^{\circ}$  and  $35^{\circ}$ S) in FRAM, and these may be compared to [Figs. 3a and 3b](#) here. (Note that the streamfunctions in [Fig. 3](#) are for the effective transport velocity, but these here differ little from the corresponding streamfunctions for the Eulerian-mean velocity.) The FRAM model features a very strong southward outflow of more than 18 Sv in the Atlantic between 1200 and 3000 m [e.g., [Fig. 3b](#) of [Döös \(1994\)](#)], whereas the GM-1 case features an outflow of only about 8 Sv ([Fig. 3a](#)). The FRAM circulation in the Indian/Pacific features a strong (12 Sv) northward inflow below about 2500 m and an equally strong outflow between 2000 and 1000 m [[Figs. 3d and 3e](#) of [Döös \(1994\)](#)]. In contrast, the GM-1 case features an abyssal inflow of 8 Sv and almost no midlevel outflow ([Fig. 3b](#)). Observational analysis (e.g., [Wunsch et al. 1983](#); [Toggweiler and Samuels 1992](#); [Wijffels et al. 1996](#)) indicate that, at least in the Pacific, most of the abyssal inflow exits southward at middepth without upwelling into the thermocline. The present model Pacific circulation is not consistent with these observations (streamfunction calculations for the Pacific alone yield a pattern very similar to that in [Fig. 3b](#)). With regard to the Atlantic circulation, the wide spread of estimates of net deep Atlantic outflow precludes discrimination between the models on that basis. However, the deep Atlantic outflow is certainly too shallow in the GM cases (e.g., [Fig. 3a](#); cf. [Martel and Wunsch 1993](#)) and this is reflected in excessive penetration of relatively fresh, cold Antarctic Bottom Water into both the deep South and North Atlantic (e.g., [Figs. 6](#) and [7](#) of [Hirst and McDougall 1996](#)). Similar problems appear evident in the GM solutions of [Large et al. \(1997\)](#) and [England and Hirst \(1997, manuscript submitted to J. Phys. Oceanogr.\)](#). The above deficiencies in the Pacific and

Atlantic-deep circulations are long standing problems in global ocean modeling, and the GM scheme alone does not appear to help. Nevertheless, we expect that schemes like GM, by permitting a more realistically low diffusion environment, will help to provide a better basis for future progress on these problems.

In a second discrepancy, the FRAM model shows a deep cell that appears totally unconnected with Antarctic surface water densities, unlike the Antarctic deep cell in [Fig. 5b](#). This lack of connection in the case of FRAM may reflect the absence of Antarctic Bottom Water formation therein, which primarily resulted from a surface restoration strategy not appropriate for the attainment of peak winter surface densities (e.g., [Döös and Webb 1994](#)).

### *b. The Deacon cell as a tracer transport agent*

There has been considerable discussion in the literature as to the significance of the near-cancellation of the Deacon cell when the effective transport velocity is averaged in height coordinates, and several authors suggest that this near cancellation eliminates the Deacon cell as a tracer transport agent. However, with or without the GM eddy transport scheme, tracer transport is not determined by the zonally averaged velocity field. Tracers are instead transported by the residual-mean circulation ([Andrews and McIntyre 1976](#)), and this has been applied to the analysis of the FRAM ocean model by [McIntosh and McDougall \(1996\)](#). The residual-mean streamfunction is the sum of the Eulerian-mean streamfunction and  $-\overline{\mathcal{V}'\rho'}/\rho_z^-$ , where the averaging operator is a zonal average and  $\rho$  stands for a relevant density variable. The zonally averaged meridional density flux  $\overline{\mathcal{V}'\rho'}$  contains not only the correlations due to mesoscale eddy variability (such as might be captured by the eddy-induced transport of the GM scheme), but also the correlations over large zonal length scales associated, for example, with the large meandering motion of the standing eddies in the ACC. The GM parameterization is not designed to account for these large-scale correlations, so we should not expect the zonal-mean of the effective transport velocity to possess the adiabatic property of the zonal residual-mean flow. While [Gent et al. \(1995\)](#) realized that the effective circulation in three dimensions is close to being along isopycnals (adiabatic), this does not mean that the zonally averaged effective velocity field should be aligned along zonally averaged isopycnals. This is apparent in [Fig. 1a](#) where our zonally averaged effective velocity field exhibits a weak Deacon cell whose strength is about one-third of the Deacon cell of the Eulerian-mean flow in [Fig. 2a](#). While the majority of the Deacon cell is canceled upon the introduction of the GM scheme under current model settings, we do not believe that this is a necessary consequence of such a scheme, and the extent of the cancellation will depend, for example, on the value of the diffusivity ( $\kappa_e$ ) used in the scheme.

## 5. Conclusions

This paper compares the meridional overturning circulation, as viewed in density coordinates, for two versions of a  $z$ -coordinate World Ocean model. Both versions include a standard profile of vertical diffusivity and isoneutral tracer diffusion via the [Cox \(1987\)](#) scheme. In addition, one version (GM) includes eddy-induced advection as per the GM scheme; the other (HB) includes a standard background horizontal diffusivity. There are some marked differences between the meridional cells evident in solutions for the two versions. The GM version displays a very simple four cell structure with cells for Antarctic overturning, for North Atlantic overturning, and the North and South subtropical gyres. The HB version displays a more complicated cell structure with the Antarctic overturning circulation split into two cells and with the appearance of a residual Deacon cell. By decomposing the dianeutral velocity field into components resulting from fluxes associated with individual mixing processes, we show that the above differences result almost entirely from the presence of horizontal diffusive fluxes in the HB version. In particular, the massive ( $>20$  Sv) upward dianeutral transport near  $60^\circ\text{S}$  in the HB version, induced there by horizontal diffusive flux, is completely absent in the GM version. The contributions of other components of dianeutral velocity remain relatively unchanged between the versions. Since horizontal diffusive fluxes are generally believed to be fictitious, their importance raises serious questions about the integrity of the HB solution. For example, the massive dianeutral transport near  $60^\circ\text{S}$  represents a severe erosion of the dense Antarctic deep waters by horizontal diffusive buoyancy flux from the north and is probably one causative factor of the host of other problems (i.e., insufficient deep density, excessive convection and ventilation, excessive implied surface heat and freshwater loss, unrealistic deep water properties) that tend to beset the Southern Oceans of horizontal-diffusive models (e.g., [England 1995](#); [Toggweiler and Samuels 1995](#); [Hirst and McDougall 1996](#)).

The level-surface and density-coordinate representations of the meridional overturning streamfunction for both model versions are compared to those of FRAM. The density-coordinate representation for both GM and FRAM do not show any Deacon cell, in contrast to HB where a residual Deacon cell is fairly pronounced. However, both the GM and HB versions show a Pacific circulation where a large volume of abyssal water upwells into the thermocline, unlike in FRAM or that inferred from observations. In the Atlantic, the GM version in particular gives a deep outflow that is too shallow, and the intrusion of Antarctic Bottom Water into the North Atlantic is too strong (see also [England and Rahmstorf 1997](#), manuscript submitted to *J. Phys. Oceanogr.*). This is despite fairly realistic density differences between the densest North Atlantic Deep Water and the Antarctic Bottom Water ([Hirst and McDougall 1996](#)).

There has been substantial recent progress in refining the tracer advection and diffusion numerics in  $z$ -coordinate ocean models. The improved isoneutral diffusion scheme of [Griffies et al. \(1998\)](#) higher-order schemes for tracer advection in models of moderately high resolution (e.g., [Gent et al. 1998](#)) and explicit parameterizations of sill overflow (e.g., [Beckmann and Döschner 1997](#)) together offer the possibility of models achieving fairly realistic levels of dianeutral diffusion without recourse to the GM scheme. In such a model with no GM scheme, we see no reason for any fundamental change from the basic four cell structure of meridional overturning evident in [Figs. 5a,b](#). In any case, the GM scheme parameterizes an important physical process, namely, loss of mean-state available potential energy as a result of baroclinic eddy activity, so it, or some similar scheme, is required irrespective of its beneficial effects on the model numerics. A major potential benefit of

the other recent model improvements is that values of model coefficients such as  $\kappa_e$ ,  $\kappa_i$ , and  $\kappa_v$  might no longer be severely constrained for numerical reasons, and so may be set on the basis of physical consideration.

### Acknowledgments

The authors would like to thank Drs. Peter McIntosh, Richard Matear, Jurgen Willebrand, and Peter Gent and an anonymous reviewer for their comments on earlier versions of the manuscript. The computations were carried out on the CSIRO CRAY-YMP4E/369 at the University of Melbourne, Parkville, Victoria. This work is a contribution to the CSIRO Climate Change Research Program.

---

### REFERENCES

- Andrews, D. G., and M. E. McIntyre, 1976: Planetary waves in horizontal and vertical shear: The generalized Eliassen–Palm relation and the zonal mean acceleration. *J. Atmos. Sci.*, **33**, 2031–2048. [Find this article online](#)
- Beckmann, A., and R. Döscher, 1997: A method for improved representation of dense water spreading over topography in geopotential-coordinate models. *J. Phys. Oceanogr.*, **27**, 581–591..
- Böning, C. W., W. R. Holland, F. O. Bryan, G. Danabasoglu, and J. C. McWilliams, 1995: An overlooked problem in model simulations of the thermohaline circulation and heat transport in the Atlantic Ocean. *J. Climate*, **8**, 515–523. [Find this article online](#)
- Bryan, K., 1984: Accelerating the convergence to equilibrium of ocean-climate models. *J. Phys. Oceanogr.*, **14**, 666–673..
- and L. J. Lewis, 1979: A water mass model of the world ocean. *J. Geophys. Res.*, **84**, 347–376..
- Cox, M. D., 1984: A primitive-equation, 3-dimensional model of the ocean. GFDL Ocean Group Tech. Rep. No. 1, GFDL/Princeton University, Princeton, N.J., 141 pp..
- 1987: Isopycnal diffusion in a  $z$ -coordinate ocean model. *Ocean Modelling* (unpublished manuscripts), **74**, 1–5..
- Cummins, P. F., G. Holloway, and A. E. Gargett, 1990: Sensitivity of the GFDL ocean model to a parameterization of vertical diffusion. *J. Phys. Oceanogr.*, **20**, 817–830..
- Danabasoglu, G., and J. C. McWilliams, 1995: Sensitivity of the global ocean circulation to parameterizations of mesoscale tracer transports. *J. Climate*, **8**, 2967–2987. [Find this article online](#)
- — and P. R. Gent, 1994: The role of mesoscale tracer transports in the global ocean circulation. *Science*, **264**, 1123–1126..
- Döös, K., 1994: Semianalytical simulation of the meridional cells in the Southern Ocean. *J. Phys. Oceanogr.*, **24**, 1281–1293..
- 1996: The meridional circulation in the Southern Ocean and its seasonal variability as seen by the Fine-Resolution Antarctic Model. *J. Geophys. Res.*, **101** (C3), 6393–6407..
- and D. J. Webb, 1994: The Deacon cell and the other meridional cells of the Southern Ocean. *J. Phys. Oceanogr.*, **24**, 429–442..
- England, M. H., 1993: On the formation of global-scale water masses in ocean general circulation models. *J. Phys. Oceanogr.*, **23**, 1523–1552..
- 1995: Using chlorofluorocarbons to assess ocean climate models. *Geophys. Res. Lett.*, **22**, 3051–3054..
- and A. C. Hirst, 1997: Chlorofluorocarbon uptake in a world ocean model. 2: Sensitivity to surface thermohaline forcing and subsurface mixing parameterization. *J. Geophys. Res.*, **102**, 15 709–15 731..
- Gent, P. R., and J. C. McWilliams, 1990: Isopycnal mixing in ocean circulation models. *J. Phys. Oceanogr.*, **20**, 150–155..
- and — 1996: Eliassen–Palm fluxes and the momentum equations in non-eddy-resolving ocean circulation models. *J. Phys. Oceanogr.*, **26**, 2539–2546..
- J. Willebrand, T. J. McDougall, and J. C. McWilliams, 1995: Parameterizing eddy-induced tracer transports in ocean circulation models. *J. Phys. Oceanogr.*, **25**, 463–474..
- F. O. Bryan, G. Danabasoglu, S. C. Doney, W. R. Holland, W. G. Large, and J. C. McWilliams, 1998: The NCAR climate system model global ocean component. *J. Climate*, **11**, 1287–1306. [Find this article online](#)
- Gerdes, R., C. Koberle, and J. Willebrand, 1991: The influence of numerical advection schemes on the results of ocean general circulation models. *Climate Dyn.*, **5**, 211–226..
- Gough, W. A., and C. A. Lin, 1995: Isopycnal mixing and the Veronis effect in an ocean general circulation model. *J. Mar. Res.*, **53**, 183–199..

- Griffies, S. M., A. Gnanadesikan, R. C. Pacanowski, V. Lariichev, J. K. Kowicz, and R. D. Smith, 1998: Isonutral diffusion in a  $z$ -coordinate ocean model. *J. Phys. Oceanogr.*, **28**, 805–830..
- Hellerman, S., and M. Rosenstein, 1983: Normal monthly wind stress over the World Ocean with error estimates. *J. Phys. Oceanogr.*, **13**, 1093–1104..
- Hirst, A. C., and W. Cai, 1994: Sensitivity of a World Ocean GCM to changes in subsurface mixing parameterization. *J. Phys. Oceanogr.*, **24**, 1256–1279..
- and T. J. McDougall, 1996: Deep-water properties and surface buoyancy flux as simulated by a  $z$ -coordinate model including eddy-induced advection. *J. Phys. Oceanogr.*, **26**, 1320–1343..
- , D. R. Jackett, and T. J. McDougall, 1996: The meridional overturning cells of a World Ocean model in neutral density coordinates. *J. Phys. Oceanogr.*, **26**, 775–791..
- Jackett, D. R., and T. J. McDougall, 1997: A neutral density variable for the world's oceans. *J. Phys. Oceanogr.*, **27**, 237–263..
- Jacobs, S. S., R. G. Fairbanks, and Y. Horibe, 1985: Origin and evolution of water masses near the Antarctic continental margin: Evidence from  $H^{18}_2O/H^{16}_2O$  ratios in seawater. *Oceanology of the Antarctic Continental Shelf*, S. S. Jacobs, Ed., Antarctic Research Series, Vol. 43, American Geophysical Union, 59–85..
- Killworth, P. D., and M. M. Nanneh, 1994: Isopycnal momentum budget of the Antarctic Circumpolar Current in the Fine Resolution Antarctic Model. *J. Phys. Oceanogr.*, **24**, 1201–1223..
- Large, W. G., G. Danabasoglu, S. C. Doney, and J. C. McWilliams, 1997: Sensitivity to surface forcing and boundary layer mixing in a global ocean model: Annual-mean climatology. *J. Phys. Oceanogr.*, **27**, 2418–2447..
- Levitus, S., 1982: *Climatological Atlas of the World Ocean*. NOAA Prof. Paper No. 13., U.S. Govt. Printing Office, Washington D.C., 173 pp..
- Manabe, S., R. J. Stouffer, M. J. Spelman, and K. Bryan, 1991: Transient responses of a coupled ocean–atmosphere model to gradual changes of atmospheric carbon dioxide. Part I: Annual mean response. *J. Climate*, **4**, 785–818.. [Find this article online](#)
- Martel, F., and C. Wunsch, 1993: The North Atlantic circulation in the early 1980's—An estimate from inversion of a finite-difference model. *J. Phys. Oceanogr.*, **23**, 898–924..
- McDougall, T. J., 1987a: Neutral surfaces. *J. Phys. Oceanogr.*, **17**, 1950–1964..
- , 1987b: Thermobaricity, cabbeling and water-mass conversion. *J. Geophys. Res.*, **92**, 5448–5464..
- , 1991: Parameterizing mixing in inverse models. *Dynamics of Oceanic Internal Gravity Waves*, P. Muller and D. Henderson, Eds., *Proc. Sixth 'Aha Huliko'a Hawaiian Winter Workshop*, University of Hawaii at Manoa, HI, 355–386..
- and J. A. Church, 1986: Pitfalls with the numerical representation of isopycnal and diapycnal mixing. *J. Phys. Oceanogr.*, **16**, 196–199..
- and P. C. McIntosh, 1996: The temporal-residual-mean velocity. Part I: Derivation and the scalar conservation equations. *J. Phys. Oceanogr.*, **26**, 2653–2665..
- , A. C. Hirst, M. H. England, and P. C. McIntosh, 1996: Implications of a new eddy parameterization for ocean models. *Geophys. Res. Lett.*, **23**, 2085–2088..
- McIntosh, P. C., and T. J. McDougall, 1996: Isopycnal averaging and the residual mean circulation. *J. Phys. Oceanogr.*, **26**, 1655–1660..
- McWilliams, J. C., G. Danabasoglu, and P. R. Gent, 1996: Tracer budgets in the warm water sphere. *Tellus*, **48**, 179–192..
- Redi, M. H., 1982: Oceanic isopycnal mixing by coordinate rotation. *J. Phys. Oceanogr.*, **12**, 1154–1158..
- Reid, J. L., 1994: On the total geostrophic circulation of the North Atlantic Ocean: Flow patterns, tracers and transports. *Progress in Oceanography*, Vol. 33, Pergamon, 1–92..
- Toggweiler, J. R., and B. Samuels, 1992: New radio carbon constraints on the upwelling of abyssal water to the ocean's surface *The Global Carbon Cycle*, M. Heimann, Ed., NATO ASI Series, Springer, 333–366..
- and B. Samuels, 1995: Effect of sea ice on the salinity of Antarctic Bottom Waters. *J. Phys. Oceanogr.*, **25**, 1980–1997..
- Veronis, G., 1975: The role of models in tracer studies. *Numerical Models of the Ocean Circulation*, Natl. Acad. Sci., 133–146..
- Wijffels, S. E., J. M. Toole, H. L. Bryden, R. A. Fine, W. J. Jenkins, and J. L. Bullister, 1996: The water masses and circulation at 10°N in the Pacific. *Deep-Sea Res.*, **43**, 501–544..
- Williams, R. G., M. A. Spall, and J. C. Marshall, 1995: Does Stommel's mixed layer “Demon” work? *J. Phys. Oceanogr.*, **25**, 3089–3102..



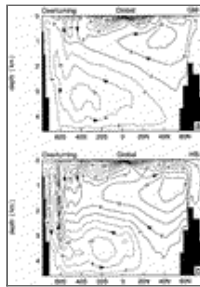
## Tables

Table 1. Differences between the four model runs. Values of parameters  $\kappa_h$ ,  $\kappa_e$ , and  $\kappa_i$  for each run, with units of  $10^7 \text{ cm}^2 \text{ s}^{-1}$ , and dash indicating zero value. Also shown are the  $e$ -folding timescale (in days) for the surface restoration (“ $\gamma^{-1}$ ”), and whether restoration salinity is enhanced near Antarctica (under “Antarctic salt”).

Run	$\kappa_h$	$\kappa_e$	$\kappa_i$	$\gamma^{-1}$	Antarctic salt
HB-1	0.7	—	1	4	Yes
GM-1	—	1	1	15	No
HB-2	0.7	—	1	30	No
GM-2	—	1	1	30	No

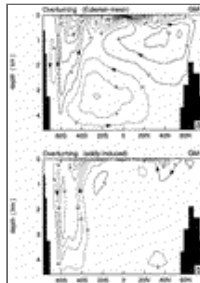
[Click on thumbnail for full-sized image.](#)

## Figures



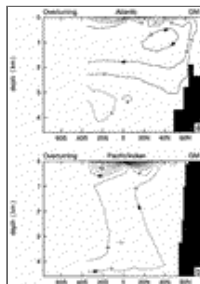
[Click on thumbnail for full-sized image.](#)

Fig. 1. Meridional overturning streamfunction  $\Psi(\lambda, z)$  for level-surface integration of the effective transport velocity zonally about the globe, in runs (a) GM-1 and (b) HB-1. Contours are at 4-Sv intervals. Dashed contours indicate negative values of streamfunction.



[Click on thumbnail for full-sized image.](#)

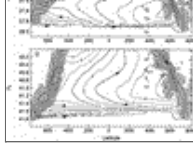
Fig. 2. Meridional overturning streamfunction  $\Psi(\lambda, z)$  for level-surface integration (a) the Eulerian-mean and (b) the eddy-induced transport velocity components, in run GM-1. Otherwise as for [Fig. 1](#).



[Click on thumbnail for full-sized image.](#)

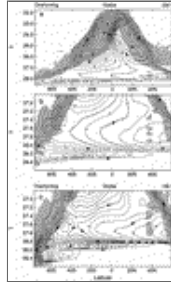
Fig. 3. Meridional overturning streamfunction  $\Psi(\lambda, z)$  for level-surface integration of the effective transport velocity across (a) the Atlantic and (b) the Pacific/Indian Oceans, in run GM-1. Otherwise as for [Fig. 1](#).





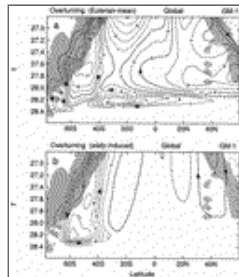
[Click on thumbnail for full-sized image.](#)

Fig. 4. Meridional overturning streamfunctions of the effective transport velocity in run GM-1, where the zonal integration is performed about the globe along potential density surfaces; (a)  $\Psi(\lambda, \sigma_\theta)$  (full density range), (b)  $\Psi(\lambda, \sigma_\theta)$  (high density range only), and (c)  $\Psi(\lambda, \sigma_3)$  (high density range only). Contour interval in (a) is 4 Sv and in (b) and (c) is 2 Sv. Shading indicates range of potential densities found at the surface at each latitude. Also, shading near 37°N indicates densities at subsurface Atlantic Ocean points adjacent to Gibraltar into which Mediterranean Water is mixed. [The model includes a Mediterranean Sea, and the effect of its outflow on the Atlantic is parameterized via an exchange of tracers at a prescribed rate between adjacent grid points across the (unresolved) Gibraltar Strait (see [Hirst and McDougall 1996](#)).]



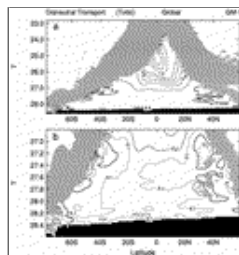
[Click on thumbnail for full-sized image.](#)

Fig. 5. Meridional overturning streamfunction  $\Psi(\lambda, \gamma)$ , where the zonal integration is performed along neutral surfaces as computed via the method of [Jackett and McDougall \(1997\)](#), for (a) full and (b) high  $\gamma$  range of GM-1 and (c) high  $\gamma$  range of HB-1. Otherwise as for [Fig. 4](#).



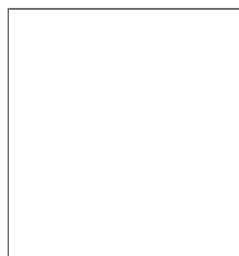
[Click on thumbnail for full-sized image.](#)

Fig. 6. Meridional overturning streamfunction  $\Psi(\lambda, \gamma)$  for (a) Eulerian-mean and (b) eddy-induced velocity components. Only high  $\gamma$  range shown. Otherwise as for [Fig. 4](#).



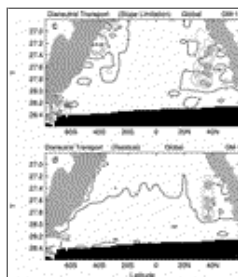
[Click on thumbnail for full-sized image.](#)

Fig. 7. Subsurface dianeutral transport zonally integrated along the neutral surfaces, calculated via (3c). Units of dianeutral transport are Sverdrups per degree latitude, and contours are at 0,  $\pm 0.1$ ,  $\pm 0.2$ ,  $\pm 0.4$ ,  $\pm 0.6$ ,  $\pm 0.8$ ,  $\pm 1.0$ ,  $\pm 1.5$ , . . . units. Dashed contours indicate negative values (i.e., downward dianeutral transport).



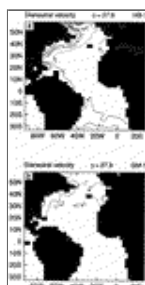
[Click on thumbnail for full-sized image.](#)

Fig. 8. Components of dianeutral transport resulting from (a) vertical diffusion, (b) isoneutral tracer diffusion, (c) slope limitation of isoneutral tracer diffusion scheme, and (d) residual. Components (a)–(c) calculated directly from the respective term on the right-hand side of (4). Otherwise as in Fig. 7. Contours  $\pm 0.05$  Sv per degree latitude are also shown in (b)–(d).



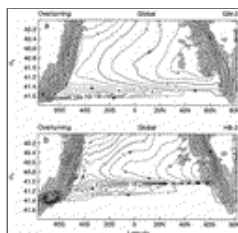
[Click on thumbnail for full-sized image.](#)

Fig. 8. (Continued)



[Click on thumbnail for full-sized image.](#)

Fig. 9. Dianeutral velocity component  $e$  across the  $\gamma = 27.9$  neutral surface in the Atlantic Ocean in (a) HB-1 and (b) GM-1 for  $e$  calculated as indicated in (3c). Units of dianeutral velocity are  $10^{-6} \text{ m s}^{-1}$  with contours at  $\pm 0.1, \pm 0.5, \pm 1.5, \pm 2.5, \dots$  units. Dashed contours indicate negative values (i.e., downward dianeutral transport). Black shading indicates land, dark gray shading indicates bottom  $\gamma < 27.9$ , and light shading indicates ocean surface  $\gamma > 27.9$ .



[Click on thumbnail for full-sized image.](#)

Fig. 10. Meridional overturning streamfunction  $\Psi(\lambda, \sigma_3)$  in runs (a) GM-2 and (b) HB-2. Only high density range shown. Otherwise as in Fig. 4.

Corresponding author address: Dr. Anthony C. Hirst, CSIRO Division of Atmospheric Research, Private Bag No. 1, Aspendale, Victoria 3195, Australia.

E-mail: [ach@dar.csiro.au](mailto:ach@dar.csiro.au)

<sup>1</sup> Except where noted, the term “transport” herein refers to the integrated volume flux of the advecting velocity across a surface and has units of Sverdrups ( $1 \text{ Sv} \equiv 10^6 \text{ m}^3 \text{ s}^{-1}$ ).

<sup>2</sup> For example, deep water potential densities in both cases are mostly within  $\pm 0.1 \text{ kg m}^{-3}$  of Levitus (1982) values.

<sup>3</sup> HJM actually evaluate a slightly simpler form, obtained from (3c) by taking the small slope limit. In practice, the integrand of the two forms varies by less than 1% for slopes less than 1:10, and we find that the two forms give almost identical results for Figs. 7 and 8.



© 2008 American Meteorological Society [Privacy Policy and Disclaimer](#)  
Headquarters: 45 Beacon Street Boston, MA 02108-3693  
DC Office: 1120 G Street, NW, Suite 800 Washington DC, 20005-3826  
[amsinfo@ametsoc.org](mailto:amsinfo@ametsoc.org) Phone: 617-227-2425 Fax: 617-742-8718  
[Allen Press, Inc.](#) assists in the online publication of *AMS* journals.